Check for updates

Numerical analysis of HgCdTe dual-band infrared detector

M. Kopytko[1] · W. Gawron[2] · A. Kębłowski[2] · D. Stępień[2] · P. Martyniuk[1] ·
K. Jóźwikowski[1]

Abstract

In this paper we describe recent progress in the HgCdTe multilayer heterostructures grown by metaloorganic chemical vapour deposition on GaAs substrates for photodetectors operated above 200 K. We present example of design and characterization of the new classical N^+–n–P^+–p–N^+ back to back HgCdTe dual-band photodiode structure, that operates within the mid-wavelength infrared band in sequential mode. A numerical modelling was used for investigation of the device design on the current responsivity and dark currents. The program based on the solution of the system of the carrier transport equations including the whole spectrum of various generation and recombination mechanisms consisting of Shockley–Read–Hall, Auger and radiative generation-recombination terms. Additionally, tunneling effects such as band-to-band and trap-assisted tunnelling models are included in the continuity equations by incorporating them as additional generation–recombination processes.

Keywords Numerical modelling · Dual-band infrared detector · Generation-recombination processes

1 Introduction

Two-color detectors have the ability to detect two different infrared (IR) bands or two different wavelengths in the same band separately and independently. Dual-band detection can greatly improve overall system performance: it provides an additional dimension of

✉ M. Kopytko
   malgorzata.kopytko@wat.edu.pl

1 Institute of Applied Physics, Military University of Technology, 2 Urbanowicza St.,
   00-908 Warsaw, Poland

2 Vigo System S.A., 129/133 Poznańska St., 05-850 Ożarów Mazowiecki, Poland

contrast that is available for signal processing allowing determination of the temperature of the scene, assuming constant emissivity in the entire spectral range (Rogalski 2005).
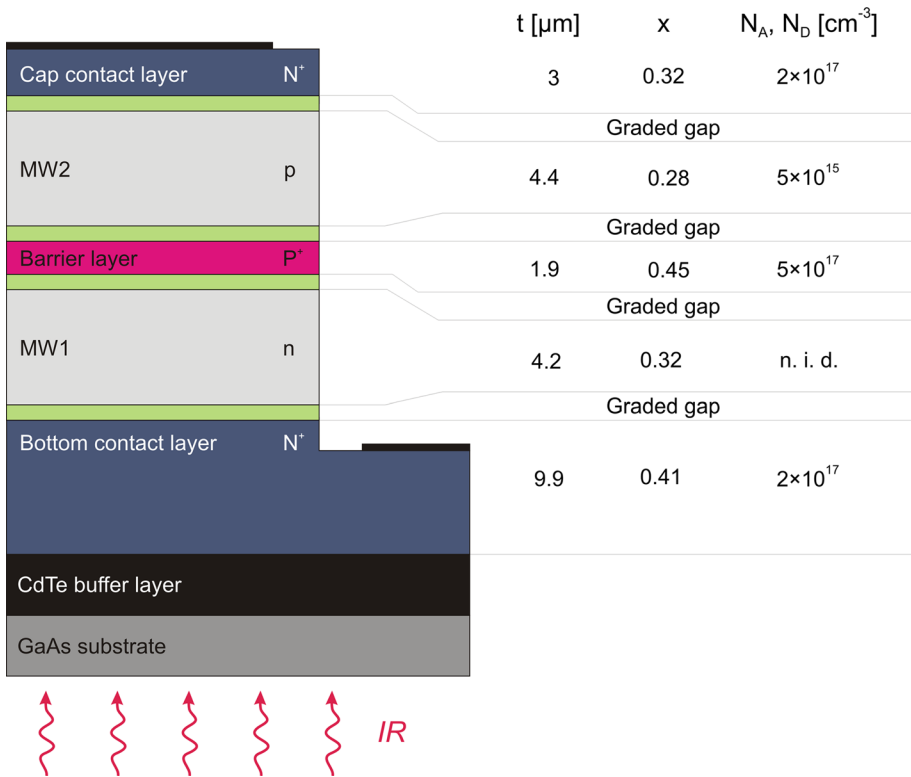
The architecture of the device is implemented in such a way that the long-range photodiode is placed physically directly behind the photodiode at shorter wavelengths. Such detector can operate in sequential or simultaneous modes. The sequential-mode detector has a single indium bump per unit cell that permits sequential bias selectivity of the spectral bands associated with operating back-to-back photodiodes. Alternatively simultaneous detector typically contain multiple electrical contact per unit cell and are grounded through the substrate on which detector is grown. Photosignal is extracted directly from one of contacts, while the second contact, common to both spectral bands, provides the sum of the two photocurrents. While this architecture provides the benefit of real-time imaging, the geometry of the pixel reduces the optical fill factor and reduces the maximum achievable quantum efficiency. The challenges involved with fabricating arrays having multiple contacts per unit cell further limit the development of simultaneous detectors. For the above reason sequential detectors have emerged as the favoured two-color technology.

The HgCdTe alloy is an ideal material for producing dual-band IR structures. It exhibits a wavelength cut-off proportional to the alloy composition and offer multi-colour capability in the short wave infrared (SWIR), middle wave infrared (MWIR) and long wave infrared (LWIR) ranges. Two-colour detectors using HgCdTe photoconductors have been demonstrated in the early 1970s (Halpert and Musicant 1972). As molecular beam epitaxy (MBE) and metaloorganic chemical vapour deposition (MOCVD) techniques developed, considerable efforts have been directed to fabricating multilayer heterostructures with excellent control of composition and doping profiles. The simplest n–P–N triple-layer heterojunction (TLHJ) back-to-back photodiode operating in the bias-selectable mode was reported by Raytheon (Wilson et al. 1994; Smith et al. 2011). The same mode with more complicate n–p–P–p–n architecture and was proposed by Leti (Ballet et al. 2004) and later by Shanghai Institute of Technical Physics (Hu et al. 2014). Simultaneous mode has been achieved in a number of ingenious architectures: n–p–n design by Raytheon (Rajavel et al. 1998) p–n–N–p–n BAE System (Reine et al. 1998), n–p–P–p–n Leti (Zanatta et al. 2000) and structures based on p-on-n or n-on-p junction—Rockwell (Tennant et al. 2001) and Leti (Destefanis et al. 2007) respectively.

2 Device design

The investigated bias-selectable two-colour HgCdTe detector adopts a multi-layer heterostructure grown by MOCVD. The growth has been carried out in Aixtron AIX-200 system on 2 inch, epiready, semi-insulating (100) GaAs substrates, oriented 2° off toward nearest <110> using the interdiffused multilayer process (IMP) technique (Svoronos et al. 1996).

Device architecture is a simplified configuration of N^+–n–P^+–p–N^+ (where lower case letters refer to the absorber regions, while upper case letters refer to higher Cd mole fraction layers, symbol "+" denotes strong doping) as presented in Fig. 1. The detector consists of two back-to-back photodiodes. Both photodiodes detect in the MWIR spectral band, with responds between 3.0 and 4.2 µm for the first wave band and between 4.2 and 5.2 µm for the second band. For a photodiode of a more short-wave range, the active area (MW1) is a layer of non-intentionally doped (n.i.d.) material. Due to the residual background concentration at 1×10^{15} cm^{-3}, the first absorber is characterized by the n-type conductivity. In a more long-wave photodiode the active area (MW2) is the p-type layer doped with arsenic

			t [µm]	x	N_A, N_D [cm^{-3}]
Cap contact layer	N$^+$		3	0.32	2×10^{17}
		Graded gap			
MW2	p		4.4	0.28	5×10^{15}
		Graded gap			
Barrier layer	P$^+$		1.9	0.45	5×10^{17}
		Graded gap			
MW1	n		4.2	0.32	n. i. d.
		Graded gap			
Bottom contact layer	N$^+$		9.9	0.41	2×10^{17}
CdTe buffer layer					
GaAs substrate					

IR

Fig. 1 Cross-section scheme of a HgCdTe two-color IR detector

at the level of 5×10^{15} cm^{-3}. First absorber with a Cd molar composition of 0.32 act as an optical window for IR radiation reaching the second absorber with a Cd molar composition of 0.28. Both absorbing layers are separated by the barrier doped with arsenic at the level of 5×10^{17} cm^{-3} and adjustable thickness, and composition. Contacts are created to the wide-bandgap n-type layers doped with iodine at the level of 2×10^{17} cm^{-3}. By switching the bias voltage from a negative to a positive value, it is possible to detect the signal in first or the second absorber.

At the layer interfaces are the *x*-graded regions created by interdiffusion processes during HgCdTe growth at 350 °C. Compositional gradients were introduced to reduce the influence of misfit dislocations, mainly at the heterojunctions.

3 Results

Figure 2 shows the spectral photoresponse for the integrated HgCdTe two-colour IR detector illustrated in Fig. 1, where the corresponding two spectral bands with cut-off wavelengths of 4.1 µm and 5.05 µm at 230 K are evident. At 300 K, the cut-off wavelengths move at 3.9 µm and 4.7 µm, respectively. The cut-off wavelength of the MW1 photodiode is close to the cut-on wavelength of the MW2 diode. The simulated spectral photoresponse is also compared to that of experimental results showing that the simulation and

Fig. 2 Measured (points) and simulated (lines) spectral photoresponse of HgCdTe Dual-band IR detector operated at 230 K (**a**) and 300 K (**b**). A voltage of ±0.1 V has been used in the simulation and experiment
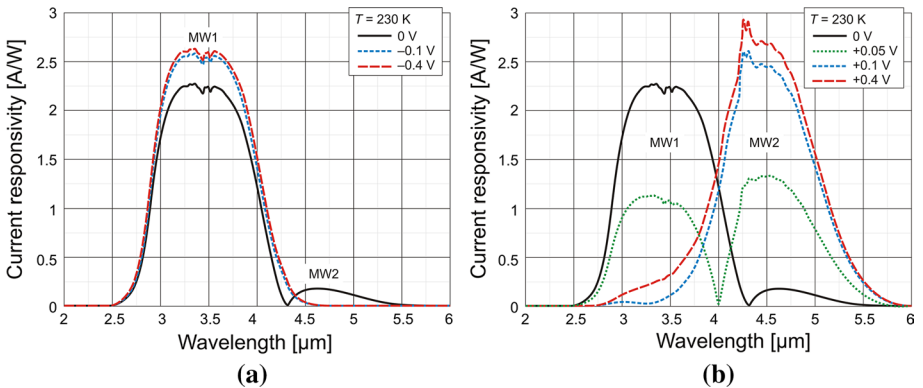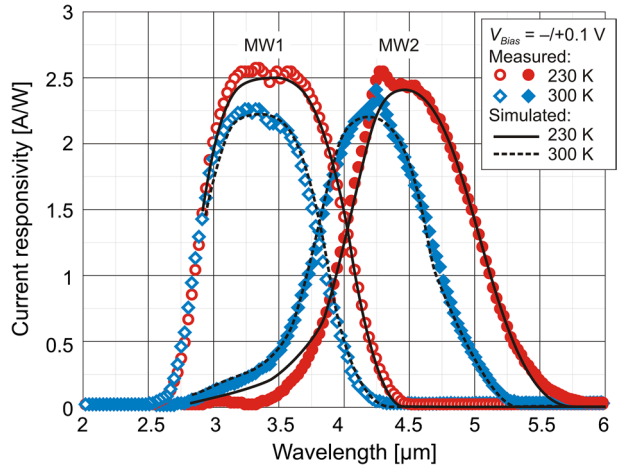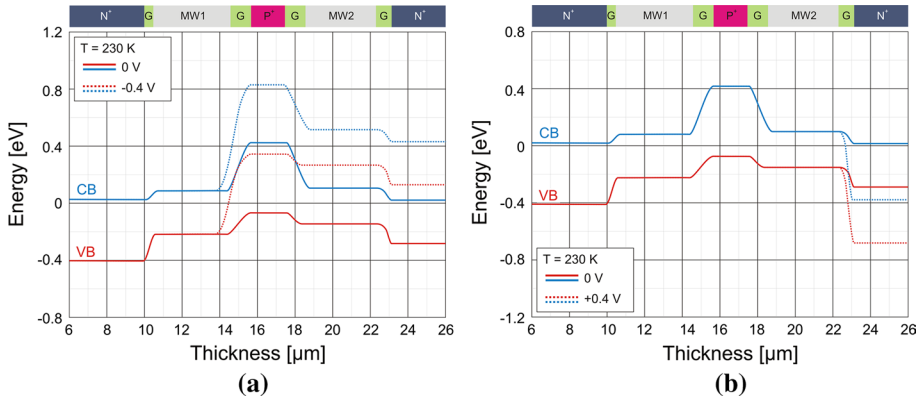

Fig. 3 Measured spectral photoresponse of HgCdTe dual-band IR detector operated at 230 K and under a negative (**a**) and a positive (**b**) bias voltage

experiment are in good agreement. The ±0.1 V voltage has been chosen as optimal, at which the crosstalk between the two photodiodes is eliminated. At a zero bias voltage, a photodiode of a more short-wave range is dominant (Fig. 3). The responsivity of both photodiodes equates around +0.05 V (Fig. 3).

For the assumed molar composition and doping profiles, the calculated band diagram of the detector operated under a negative (−0.4 V) and a positive (+0.4 V) bias voltage was plotted on Fig. 4. In case of biasing the detector with −0.4 V voltage, the electric field (Fig. 5) is distributed near the MW1 absorber on the n–P$^+$ junction. When the detector is biased with +0.4 V voltage, the electric field is distributed in the area of MW2 absorber on the p–N$^+$ junction. The electric field associated with the junction areas, with an intensity of over 10^6 V cm^{-1} (Fig. 5), activates SRH mechanisms related to dislocations. As a result, the rate of thermal generation related to SRH mechanisms increases.

The current–voltage (I–V) characteristics of the photodiodes are influenced by various generation-recombination (GR) mechanisms occurred in semiconductors. One of the methods of analyzing these mechanisms is numerical modelling of theoretical

Fig. 4 Calculated band diagram of HgCdTe dual-band IR detector operated at 230 K and under a negative (**a**) and a positive (**b**) bias voltage

Fig. 5 Calculated distribution of the electric field of HgCdTe dual-band IR detector operated at 230 K and under a negative and a positive bias voltage
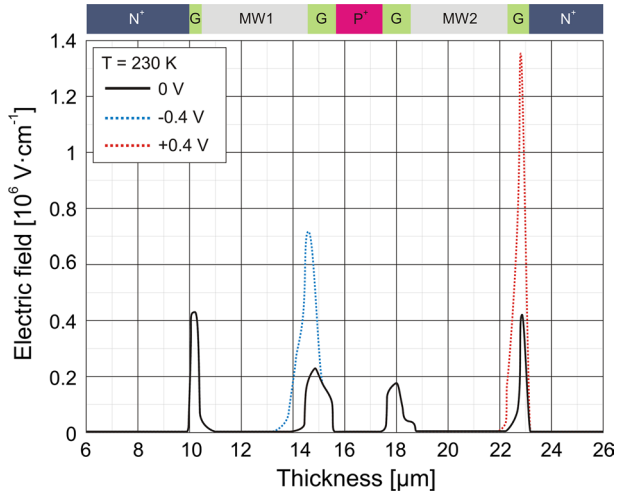
I–V characteristics and comparing them with experimental results (Jóźwikowski and Rogalski 2001; Wang et al. 2018a, b; Uzgur and Kocaman 2019). Figure 6 shows experimental I–V curves (solid lines) and theoretical curves (dashed lines) calculated for different temperatures. The calculations were made taking into account Auger, radiative and SRH mechanism occurring through trap states related to metal (mercury) vacancies and dislocations (Jóźwikowski et al. 2011a, 2012a). A description of the procedure used for the analysis and the equations describing the mentioned GR mechanisms can be found at latest paper (Kopytko et al. 2019). The assumed mercury vacancies density is $N_T = 5 \times 10^{13}$ cm^{-3} with the ionization energy of the $E_T = 0.75 E_g$ above the top of the valence band. The density of dislocations was assumed at the level of $G_{DIS} = 1 \times 10^6$ cm^{-2} with the energy of activation of the dislocation band of $E_{DIS} = 0.32 E_g$ above the top of the valence band. For a photodiode with a more long-term absorber (MW2) and higher voltages, a good agreement of the numerical results with the experimental data was obtained. The diffusion current strongly increases with
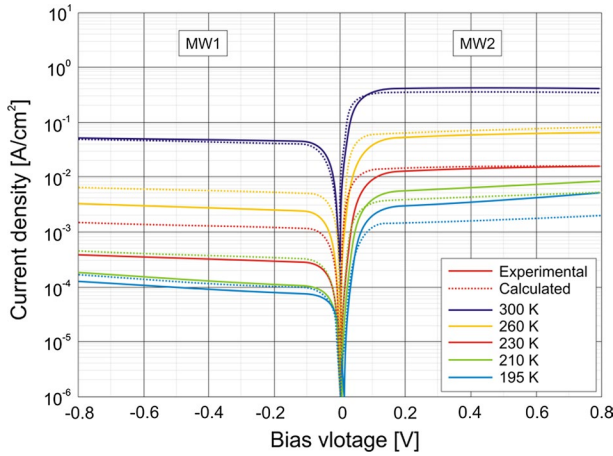
Fig. 6 Measured (solid lines) and calculated (dashed lines) current–voltage characteristics of HgCdTe dual-band IR detector

increasing temperature and the discrepancy in current values for a more short-wave photodiode (MW1) is much larger.

An additional insight of the current dependence (at the bias voltage of ± 0.2 V) of the analyzed detector on the temperature is presented in Fig. 7. The experimental results show a non-linear dependence of the dark current density in the low temperature range, especially for the MW1 photodiode. This is probably due to the presence of photocurrent originating from the background. Arrhenius plots allow us to determine the activation energy of GR processes.

For a MW2 photodiode, the specific activation energy, based on both experimental and theoretical results, is about 0.2 eV, which is smaller than the $Hg_{0.72}Cd_{0.28}Te$ bandgap at 300 K, which equals 0.264 eV. It corresponds to the value of about $0.75E_g$ and shows

Fig. 7 Arrhenius plots for HgCdTe dual-band IR detector
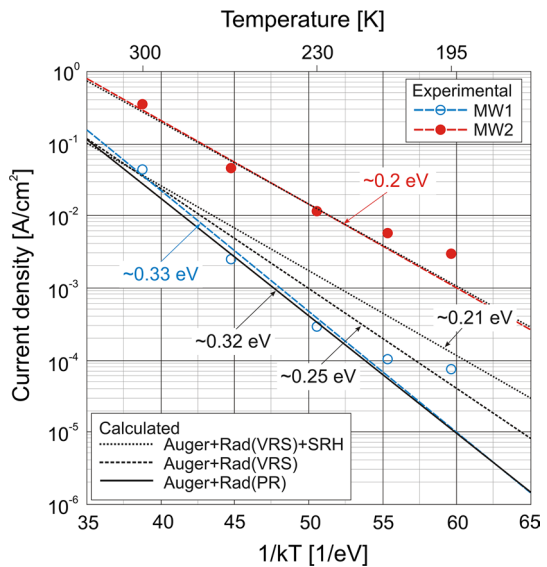
GR behaviour. For a MW1 photodiode, the activation energy of 0.33 eV determined from experimental results corresponds to the $Hg_{0.68}Cd_{0.32}Te$ bandgap, which at 300 K is 0.318 eV. Activation energy determined from theoretical calculations assuming all GR mechanisms amounts to 0.21 eV and is much smaller than the experimental one.

In order to further clarify the discrepancy, the dark current calculation for a MW1 photodiode was made for the case when the influence of the SRH mechanisms was not taken into account. In the case when the dark current is limited by the interband Auger processes and the radiative mechanism calculated using the classic Van Roosbroeck and Shockley (VRS) theory (Van Roosbroeck and Shockley 1954), the determined activation energy of 0.25 eV is larger, but still much lower than the value determined from the experimental results. Further calculations of dark currents for a MW1 photodiode were made including in the radiative recombination model the effect of photon reabsorption (PR) (Jóźwikowski et al. 2011b, 2012b). PR causes an increase in the effective carriers lifetime. The determined activation energy is 0.32 eV and is similar to the activation energy determined from the experimental results.

4 Conclusions

A numerical analysis was used to investigate the influence of different GR mechanisms on dark currents of dual-band HgCdTe detector. Results shows that a more long-wave photodiode with a p-type absorber is limited by the non-fundamental GR mechanisms related to structural defects occurring in heterostructures in the form of metal vacancies and dislocations. SRH mechanisms does not limit the parameters of the photodiodes with an n-type absorber. Shorter-wave photodiode is diffusion limited—dark currents are limited by fundamental Auger processes and radiative one. The results confirm the occurrence of the PR effect associated with radiative recombination. PR causes an increase in the effective carriers lifetime.

References

Ballet, P., Noël, F., Pottier, F., Plissard, S., Zanatta, J.P., Baylet, J., Gravrand, O., de Borniol, E., Martin, S., Castelein, P., Chamonal, J.P., Million, A., Destefanis, G.: Dual-band infrared detectors made on high-quality HgCdTe epilayers grown by molecular beam epitaxy on CdZnTe or CdTe/Ge substrates. J. Electron. Mater. **33**(6), 667–672 (2004)

Destefanis, G., Baylet, J., Ballet, P., Castelein, P., Rothan, F., Gravrand, O., Rothman, J., Chamonal, J.P., Million, A.: Status of HgCdTe bicolor and dual-band infrared focal plane arrays at LETI. J. Electron. Mater. **36**, 1031–1044 (2007)

Halpert, H., Musicant, B.I.: N-color (Hg, Cd)Te photodetectors. Appl. Opt. **11**, 2157–2161 (1972)

Hu, W., Ye, Z., Liao, L., Chen, H., Chen, L., Ding, R., He, L., Chen, X., Lu, W.: 128 × 128 long-wavelength/mid-wavelength two-color HgCdTe infrared focal plane array detector with ultralow spectral cross talk. Opt. Lett. **39**(17), 5184–5187 (2014)

Jóźwikowski, K., Rogalski, A.: Computer modeling of dual-band HgCdTe photovoltaic detectors. J. Appl. Phys. **90**, 1286–1291 (2001)

Jóźwikowski, K., Kopytko, M., Piotrowski, J., Jóźwikowska, A., Orman, Z., Rogalski, A.: Near-room temperature MWIR HgCdTe photodiodes limited by vacancies and dislocations related to Shockley–Read–Hall centers. Solid State Electron. **63**(1), 8–13 (2011a)

Jóźwikowski, K., Kopytko, M., Rogalski, A.: Numerical estimation of carrier generation-recombination processes and photon recycling effect in 3-μm n-on-p HgCdTe photodiodes. Opt. Eng. **50**, 061003 (2011b)

Jóźwikowski, K., Jóźwikowska, A., Kopytko, M., Rogalski, A., Jaroszewicz, L.R.: Simplified model of dislocations as a SRH recombination channel in the HgCdTe heterostructures. Infrared Phys. Technol. **55**(1), 98–107 (2012a)

Jóźwikowski, K., Kopytko, M., Rogalski, A.: Numerical estimations of carrier generation-recombination processes and photon recycling effect in HgCdTe heterostructure photodiodes. J. Electron. Mater. **41**, 2766–2774 (2012b)

Kopytko, M., Jóźwikowski, K., Martyniuk, P., Rogalski, A.: Photon recycling effect in small pixel p-i-n HgCdTe long wavelength infrared photodiodes. Infrared Phys. Technol. **97**, 38–42 (2019)

Rajavel, R.D., Jamba, D.M., Jensen, J.E., Wu, O.K., Wilson, J.A., Johnson, J.L., Patten, E.A., Kasai, K., Goetz, P.M., Johnson, S.M.: Molecular beam epitaxial growth and performance of HgCdTe-based simultaneous-mode two-color detectors. J. Electron. Mater. **27**, 747–751 (1998)

Reine, M.B., Hairston, A., O'Dette, P., Tobin, S.P., Smith, F.T.J., Musicant, B.L., Mitra, P., Case, F.C.: Simultaneous MW/LW dual-band MOCVD HgCdTe 64×64 FPAs. Proc. SPIE **3379**, 200–212 (1998)

Rogalski, A.: HgCdTe infrared detector material: history, status and outlook. Rep. Prog. Phys. **68**(10), 2267 (2005)

Smith, E.P.G., Venzor, G.M., Gallagher, A.M., Reddy, M., Peterson, J.M., Lofgreen, D.D., Randolph, J.E.: Large-format HgCdTe dual-band long-wavelength infrared focal-plane arrays. J. Electron. Mater. **40**(8), 1630–1636 (2011)

Svoronos, S.A., Woo, W.W., Irvine, S.J.C., Sankur, H.O., Bajaj, J.: A model of the interdiffused multilayer process. J. Electr. Mater. **25**, 1561–1569 (1996)

Tennant, W.E., Thomas, M., Kozlowski, L.J., McLevige, W.V., Edwall, D.D., Zandian, M., Spariosu, K., Hildebrandt, G., Gil, V., Ely, P., Muzilla, M., Stoltz, A., Dinan, J.H.: A novel simultaneous unipolar multispectral integrated technology approach for HgCdTe IR detectors and focal plane arrays. J. Electron. Mater. **30**, 590–594 (2001)

Uzgur, F., Kocaman, S.: Barrier engineering for HgCdTe unipolar detectors on alternative substrates. Infrared Phys. Technol. **97**, 123–128 (2019)

Van Roosbroeck, W., Shockley, W.: Photon-radiative recombination of electrons and holes in germanium. Phys. Rev. **94**, 1558–1560 (1954)

Wang, P., Wang, Y., Wu, M., Ye, Z.: A junction-level optoelectronic characterization of etching-induced damage for third-generation HgCdTe infrared focal-plane array photodetectors. Infrared Phys. Technol. **91**, 119–122 (2018a)

Wang, X., Li, Q., Zhou, S., Lin, C.: Study of dark current for LWIR HgCdTe detectors with a graded doped junction. Infrared Phys. Technol. **92**, 358–362 (2018b)

Wilson, J.A., Patten, E.A., Chapman, G.R., Kosai, K., Baumgratz, B., Goetz, P., Tighe, S., Risser, R., Herald, R., Radford, W.A., Tung, T., Terre, W.A.: Integrated two-color detection for advanced FPA applications. Proc. SPIE **2274**, 117–125 (1994)

Zanatta, J.P., Ferret, P., Loyer, R., Petroz, G., Cremer, S., Chamonal, J.P., Bouchut, P., Million, A., Destefanis, G.: Single and two colour infrared focal plane arrays made by MBE in HgCdTe. Proc. SPIE **4130**, 441–451 (2000)